Detrital epidote chemistry: detecting the alteration footprint of porphyry copper mineralization in the Quesnel terrane of the Canadian Cordillera, British Columbia

A. Plouffe[1*], P. Acosta-Góngora[1], I.M. Kjarsgaard[2], D. Petts[1], T. Ferbey[3], and K.E. Venance[1]

Plouffe, A., Acosta-Góngora, P., Kjarsgaard, I.M., Petts, D., Ferbey, T., and Venance, K.E., 2021. Detrital epidote chemistry: detecting the alteration footprint of porphyry copper mineralization in the Quesnel terrane of the Canadian Cordillera, British Columbia; in *Targeted Geoscience Initiative 5: contributions to the understanding and exploration of porphyry deposits, (ed.) A. Plouffe and E. Schetselaar; Geological Survey of Canada, Bulletin 616, p. 137–157. https://doi.org/10.4095/327988*

Abstract: Epidote from detrital sediments derived from propylitic alteration associated with porphyry copper mineralization could be used as a vector for mineral exploration in drift-covered areas; however, differentiating porphyry-related epidote from other sources is crucial. We analyzed the composition of epidote from granitoids associated with porphyry copper mineralization, Nicola Group rocks and grains from till at three sites (Gibraltar, Mount Polley, and Woodjam) within British Columbia's Quesnel terrane, where two main sources of epidote in till are propylitic-altered rocks associated with porphyry mineralization and metamorphosed Nicola Group mafic volcanic and sedimentary rocks. Although principal component analysis was insufficient to distinguish between intrusive- and metamorphic-related epidote, patterns in the abundance of sets of elements indicate provenance. Epidote from granitoids typically has less Hf+Th (<6 ppm) and Sc+Cr+Y (<100 ppm) compared to epidote from Nicola Group rocks; abundances of As and Sb (>>4 ppm As and >>0.6 ppm Sb) in epidote derived from hydrothermal alteration zones associated with porphyry copper mineralization exceed levels measured in metamorphic epidote; and elevated Cu (approximately >30 ppm) in epidote can indicate copper mineralization. These trends in the chemical composition of till-derived epidote can be used in mineral exploration to detect buried hydrothermal alteration associated with porphyry copper mineralization.

Résumé: Dans les régions couvertes de sédiments glaciaires, l'épidote contenue dans des sédiments détritiques qui a été produite par une altération propylitique associée à une minéralisation porphyrique de cuivre pourrait servir de vecteur en exploration minérale. Il est toutefois essentiel de différencier l'épidote des systèmes porphyriques de celle provenant d'autres sources. Nous avons analysé la composition de l'épidote contenue dans des granitoïdes associés à une minéralisation porphyrique de cuivre, des roches du Groupe de Nicola et des grains provenant du till à trois emplacements (Gibraltar, Mount Polley et Woodjam) du terrane de Quesnel, en Colombie-Britannique, où les deux principales sources d'épidote dans le till sont les roches altérées par une altération propylitique associée à une minéralisation porphyrique ainsi que les roches sédimentaires et les roches volcaniques mafiques métamorphisées du Groupe de Nicola. Bien que l'analyse en composantes principales n'ait pas permis de distinguer l'épidote intrusive de l'épidote métamorphique, les profils d'abondance d'ensembles d'éléments révèlent l'origine de l'épidote. L'épidote provenant de granitoïdes contient habituellement moins de Hf+Th (<6 ppm) et de Sc+Cr+Y (<100 ppm) que l'épidote présente dans des roches du Groupe de Nicola; les quantités d'arsenic et d'antimoine (>>4 ppm pour As et >>0,6 ppm pour Sb) dans l'épidote provenant de zones d'altération hydrothermale associée à une minéralisation porphyrique de cuivre dépassent les concentrations mesurées dans de l'épidote métamorphique; et une concentration élevée de Cu (environ >30 ppm) dans l'épidote peut indiquer une minéralisation de cuivre. Ces tendances dans la composition chimique de l'épidote extraite du till peuvent servir en exploration minérale à détecter une altération hydrothermale associée à une minéralisation porphyrique de cuivre enfouie.

[1]Geological Survey of Canada, 601 Booth Street, Ottawa, Ontario K1A 0E8
[2]Mineralogical Consultant, 15 Scotia Place, Ottawa, Ontario K1S 0W2
[3]British Columbia Geological Survey, British Columbia Ministry of Energy, Mines and Petroleum Resources, 1810 Blanshard Street, Victoria, British Columbia V8T 4J1
*Corresponding author: A. Plouffe (email: alain.plouffe@canada.ca)

INTRODUCTION

The Canadian Cordillera has long been known to be rich in porphyry copper mineralization (Sutherland Brown, 1976; Schroeter, 1995; Sinclair, 2007; Logan and Schroeter, 2013; Logan and Mihalynuk, 2014). Both the Quesnel and Stikine terranes, two island arcs accreted to the North American Craton, host a wealth of porphyry copper resources. Porphyry copper deposits are also found in the Wrangell terrane to the west. In British Columbia, copper accounts for 25% of the value of mineral production (Clarke et al., 2018) and in Canada, 40% of the copper production comes from porphyry deposits (Sinclair, 2007). In their assessment of porphyry copper deposits of the Canadian Cordillera, Mihalasky et al. (2011) estimate that approximately 49 000 000 t of Cu remains to be discovered in porphyry deposits. The challenge is that prospective geology of the Stikine and Quesnel terranes is poorly exposed in places; the area is covered to a large extent by glacial sediments.

The challenge of poor exposure can be tackled in part by investigating the geochemistry and mineralogy of till. At four porphyry copper study sites in south-central British Columbia — the Gibraltar, Mount Polley, and Highland Valley Copper mines and the Woodjam prospect — Hashmi et al. (2015), Plouffe and Ferbey (2015b, 2016, 2017), Ferbey et al. (2016), and Plouffe et al. (2016) have demonstrated that till composition can be used as an indicator of the presence of mineralization in the underlying bedrock. In each of these case studies, mineralization was directly exposed to glacial erosion, resulting in glacial dispersal defined by geochemical and mineralogical anomalies in till, schematically shown in Figure 1a. Detecting the presence of porphyry mineralization at a site where the main ore zone remains below the bedrock surface and has not been directly exposed to glacial erosion (Fig. 1b) is a greater challenge. In such a scenario, ore metals (e.g. copper, molybdenum, gold) or associated minerals (e.g. chalcopyrite, gold grains) from the main ore zone would not be present in detrital sediments. Identifying minerals in till that are representative of the alteration zones that surround porphyry mineralization could be key to detecting deeply buried mineralization. One advantage of looking for porphyry alteration mineralogy in detrital sediments is that the alteration halos can extend up to a few kilometres outside the ore zone; consequently, it could result in extensive alteration mineralogy halos (Fig. 1; cf. Averill, 2011). In the context of mineral exploration, this translates into large exploration targets and increases discovery potential.

Epidote is abundant and common in propylitic alteration associated with porphyry copper mineralization (Sinclair, 2007; Sillitoe, 2010) and is dispersed in till near known porphyry copper deposits (Hashmi et al., 2015; Plouffe et al., 2016; Plouffe and Ferbey, 2017). Anomalously high epidote in till might indicate buried porphyry copper mineralization, but in the absence of ore metals or minerals in the sediments (Fig. 1b), the relationship between epidote abundance and porphyry mineralization needs to be demonstrated using epidote chemistry to identify its source. The objective of our study was to use epidote chemistry to develop a porphyry copper mineral exploration method based on alteration mineralogy. The challenge of using epidote chemistry as an indicator of porphyry hydrothermal alteration in the Quesnel terrane of central British Columbia is the need to discriminate between epidote derived from porphyry hydrothermal alteration zones in intrusive rocks and epidote derived from 'background' or unmineralized sources. The dominant source of background epidote in the Quesnel terrane is the Upper Triassic Nicola Group, which includes weakly metamorphosed volcanic and volcaniclastic rocks known to contain metamorphic epidote (Greenwood et al., 1991; Panteleyev et al., 1996; Schiarizza, 2016). Nicola Group rocks located within the alteration zone of porphyry copper mineralization could also contain hydrothermal epidote. We analyzed epidote from mineralized intrusive rocks hosting porphyry copper mineralization at the Gibraltar and Mount Polley mines and at the Woodjam prospect, and epidote from the barren, Nicola Group regional host rocks using laser-ablation inductively coupled plasma mass spectrometry (LA-ICP-MS). In addition, we analyzed epidote grains in till collected within epidote dispersal trains (down-ice) and also up-ice and distal of porphyry mineralization at each study site. We demonstrate that the chemistry of epidote recovered from till at the study sites provides an indication of its provenance from hydrothermal alteration associated with porphyry copper mineralization.

GEOLOGICAL SETTING OF PORPHYRY COPPER MINERALIZATION

Most porphyry copper deposits in the Stikine and Quesnel terranes formed during two episodes. During the earlier and most prolific event, from the Late Triassic to Middle Jurassic, porphyry mineralization formed in an island arc setting prior to accretion to North America (McMillan and Panteleyev, 1995; McMillan et al., 1995, 1996; Logan, 2013). The 208 to 202 Ma time window was a particularly prolific period, during which 90% of the known porphyry copper deposits in British Columbia formed (Logan and Mihalynuk, 2014). The second episode of porphyry formation took place in a continental arc setting after accretion to North America and extended from the Late Cretaceous to the Eocene.

We conducted a geochemical study of epidote using samples from three porphyry copper study sites: 1) the Mount Polley mine, an alkalic Cu-Au-Ag deposit; 2) the Woodjam Cu-Au prospect, which has calc-alkaline affinities; and 3) the Gibraltar mine, a calc-alkaline Cu-Mo deposit (Fig. 2). All three sites are hosted in Late Triassic to Early Jurassic felsic to intermediate intrusive rocks that intrude the Nicola Group, an Upper Triassic succession of volcanic and sedimentary rocks of the Quesnel terrane. The intrusions hosting

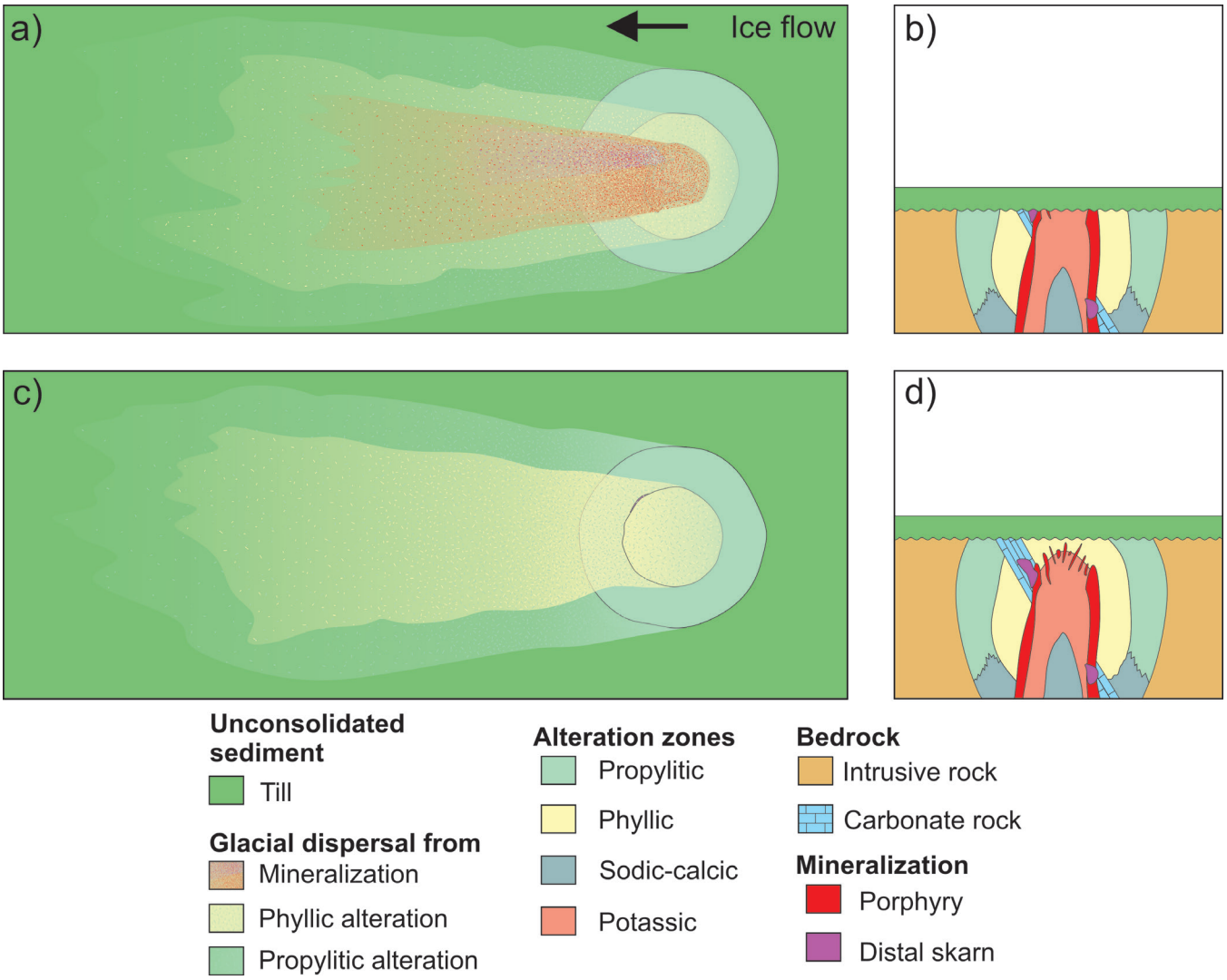

Figure 1. Schematic representation of glacial dispersal from an idealized porphyry copper deposit and associated alteration zones in a scenario with a single phase of ice movement: **a)** plan view and **b)** cross section with all alteration zones and distal skarn mineralization exposed to glacial erosion; **c)** plan view and **d)** cross section in which only the alteration zones are exposed to glacial erosion. The schematic representation of the copper deposit and alteration zones is *modified from* Lowell and Guilbert (1970) and Sillitoe (2010). The representation of the dispersal pattern is *modified from* Hickin and Plouffe (2017).

mineralization include the Mount Polley Intrusive Complex at Mount Polley (Fig. 3a), the Takomkane batholith and associated satellite intrusions at Woodjam (Fig. 3b), and the Granite Mountain batholith at Gibraltar (Fig. 3c). These deposits vary in size, with 150 000 000 t of ore grading 0.2 to 0.3% Cu and 0.2 to 0.3 g/t Au at Mount Polley (Rees, 2013), 221 000 000 t of ore grading 0.2 to 0.3% Cu and 0.3 to 0.5 g/t Au at Woodjam (Sherlock et al., 2013; Sherlock and Trueman, 2013), and 1 220 000 000 t of ore grading 0.3% Cu and 0.01% Mo at Gibraltar (van Straaten et al., 2013; Taseko Mines Ltd., 2020). Hydrothermal alteration zones with disseminated pistachio green epidote and epidote veining extend a few kilometres outward from the ore zone at each site (Drummond et al., 1976; del Real et al., 2013; Rees, 2013; Sherlock and Trueman, 2013; Kobylinski et al., 2017). A unique characteristic at Gibraltar is the presence of syn- and post-mineralization deformation, which does not occur at Mount Polley or Woodjam.

In addition to its presence in the porphyry hydrothermal alteration zones of granitoid rocks, epidote occurs in the Nicola Group rocks of the central Quesnel terrane as a result of burial metamorphism (Greenwood et al., 1991; Panteleyev et al., 1996; Ash et al., 1999). The Nicola Group rocks are dominantly composed of mafic volcanic and associated sedimentary rocks (Schiarizza, 2016). Post-mineralization regional metamorphism reached the zeolite facies at Mount Polley and Woodjam and the greenschist facies at Gibraltar (Greenwood et al., 1991; Bysouth et al., 1995; Panteleyev et al., 1996; Ash et al., 1999; Rees, 2013; van Straaten et al., 2013). The Nicola Group rocks

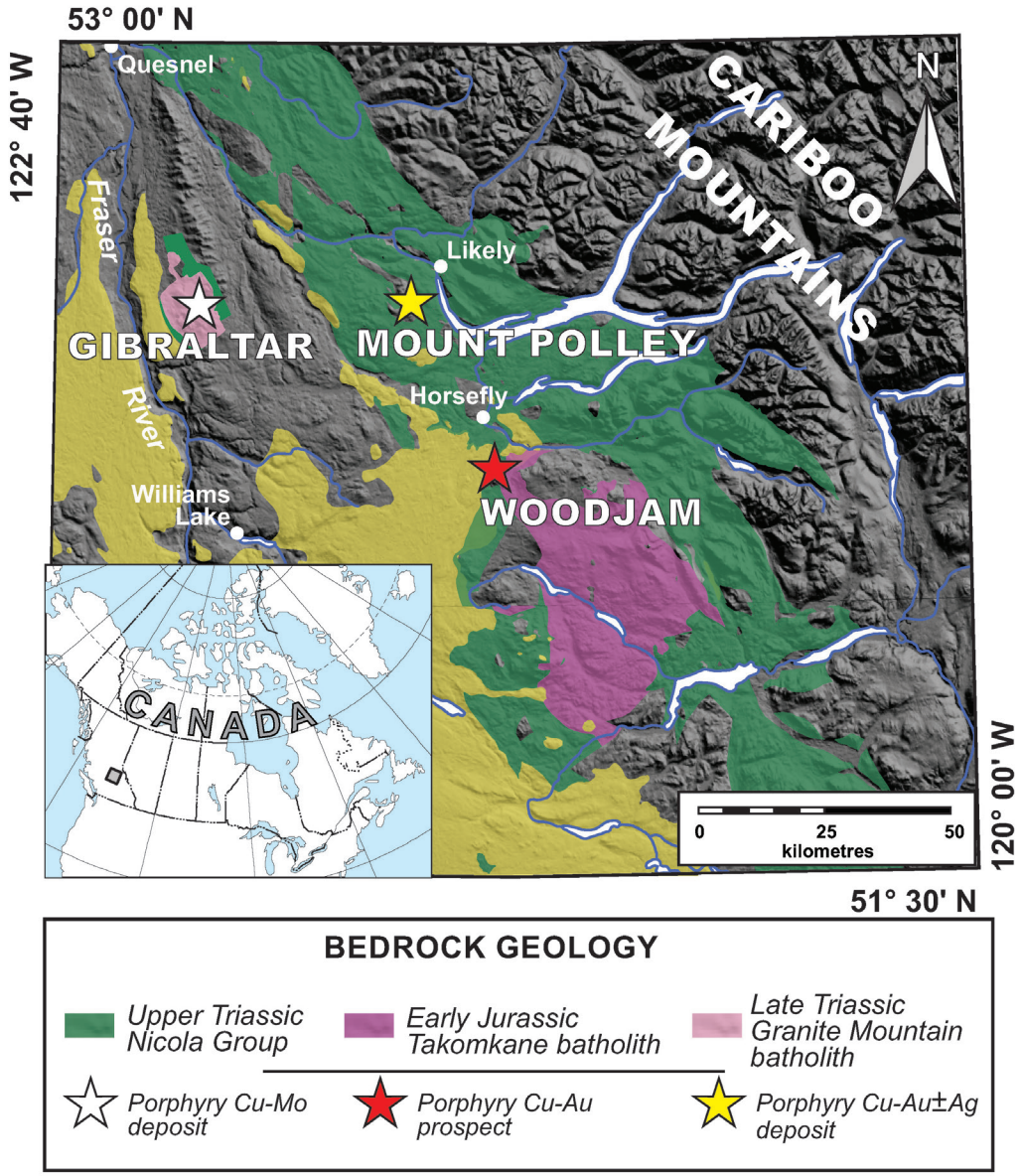

Figure 2. Location of the Gibraltar porphyry Cu-Mo deposit, the Mount Polley porphyry Cu-Au±Ag deposit and the Woodjam porphyry Cu-Au-Mo prospect in south-central British Columbia. Simplified bedrock geology *after* Massey et al. (2005), Logan et al. (2010), and Schiarizza (2019).

(Fig. 2) are the main component of the Quesnel terrane and are the dominant source of detrital epidote derived from unmineralized rocks. We sampled epidote from the Nicola Group rocks in proximity (<1 km) of and distal (>9 km) to porphyry mineralization to establish the geochemical composition of epidote derived from unmineralized rocks.

The Cordilleran Ice Sheet completely covered the three study sites during the Late Wisconsin glaciation. At Gibraltar, three phases of ice movement occurred during this glacial event: a first movement, to the southeast, related to the first glaciers that formed in a small mountain ridge with cirques and arêtes north of the mine site (Plouffe and Ferbey, 2015a); a second movement, to the southwest, derived from glaciers of the Cariboo Mountains; and a third movement, to the northwest, derived from an ice divide that formed around latitude 52°N (Plouffe et al., 2011; Plouffe and Ferbey, 2016). Only the second (southwest) and third (northwest) ice movements occurred at Mount Polley and Woodjam (Fig. 3a, b).

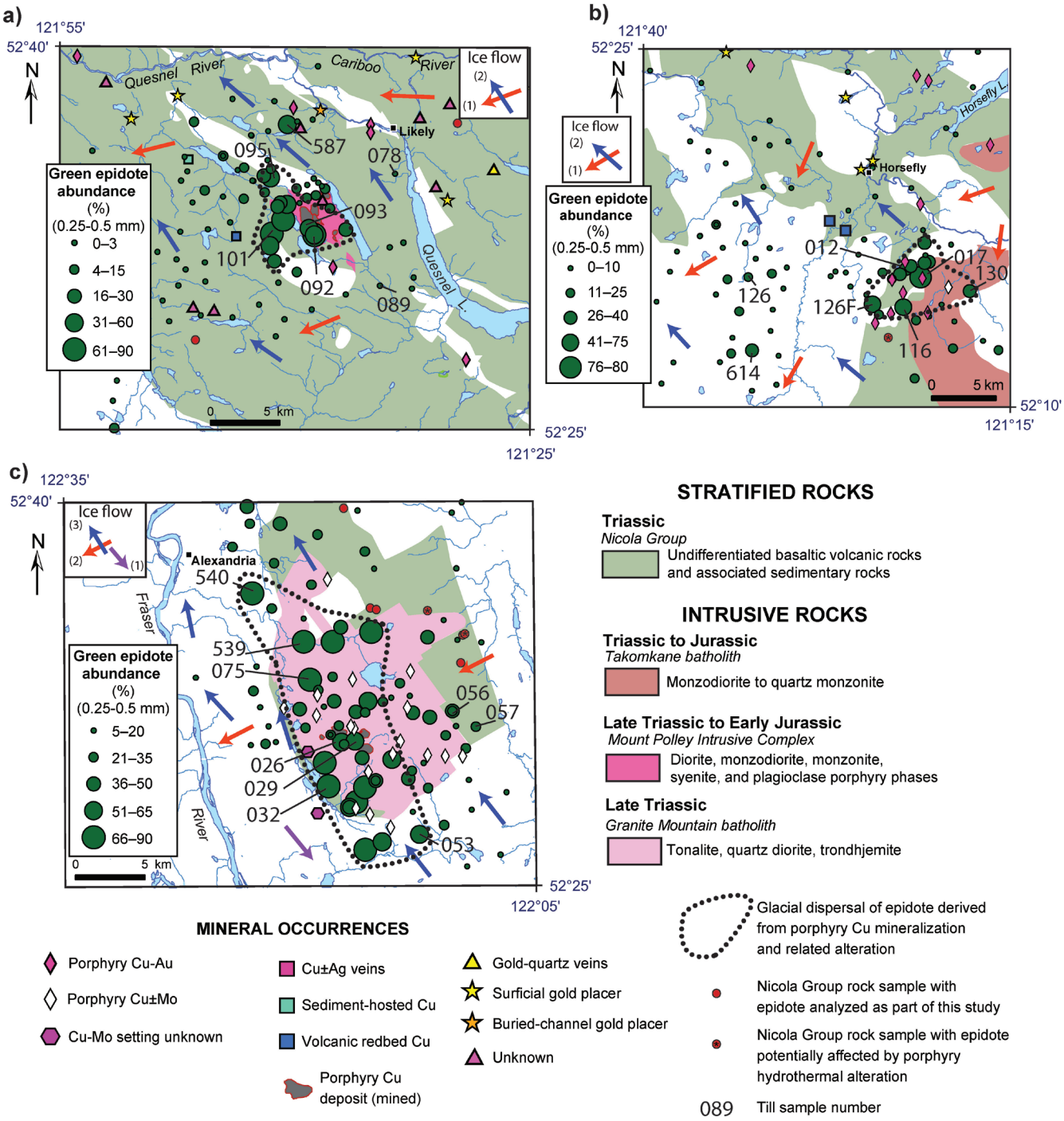

Figure 3. Abundance of green epidote in the 0.25 to 0.5 mm, greater than 3.2 SG, 0.8 to 1.0 A fraction of till samples from the **a)** Mount Polley, **b)** Woodjam, and **c)** Gibraltar occurrences in the Quesnel terrane, south-central British Columbia. The limit of glacial dispersal of epidote interpreted to be derived from porphyry copper mineralization is *modified from* Plouffe and Ferbey (2017). Ice-flow directions are *after* Plouffe and Ferbey (2016).

EPIDOTE: BACKGROUND INFORMATION AND PREVIOUS STUDIES

Minerals of the epidote supergroup are sorosilicates with the general formula $A_2M_3[T_2O_7][TO_4](O,F)(OH,O)$. Homovalent substitutions of di- and trivalent cations (e.g. Ca^{2+}, Mn^{2+}, Sr^{2+}, Pb^{2+}, or rare-earth elements $[REE]^{3+}$) can take place at the A site and trivalent cations (e.g. Al^{3+}, Fe3+, REE^{3+}) substitute in the M site, and the T site is most commonly Si (Armbruster et al., 2006). According to the classifications by Armbruster et al. (2006) and Mills et al. (2009), the epidote supergroup includes three groups: epidote, allanite (REE rich), and dollaseite (the Mg equivalent of allanite). Epidote $[Ca_2Al_2Fe^{3+}[Si_2O_7][SiO_4]O(OH)]$ and clinozoisite $[Ca_2Al_3[Si_2O_7][SiO_4]O(OH)]$ are part of the epidote group and represent the Fe- and Al-rich endmembers, respectively, of a solid solution.

Epidote is common in the propylitic alteration zone associated with porphyry systems as either a replacement product (e.g. after plagioclase) or a direct precipitate of hydrothermal fluids (e.g. in veins; Lowell and Guilbert, 1970; Sillitoe, 2010). It is also common in various metamorphic rocks from upper zeolite facies to intermediate amphibolite facies (Grapes and Hoskin, 2004), but particularly in greenschist facies. It is a mineral resistant to weathering with a hardness of 6 to 7 (Berry et al., 1983) that can withstand glacial erosion and dispersion from its bedrock source. Epidote is more abundant in till near porphyry mineralization compared to surrounding background regions, which results from glacial erosion and dispersal from epidote-bearing porphyry alteration zones (Fig. 2, 3; Hashmi et al., 2015; Plouffe et al., 2016; Plouffe and Ferbey, 2017).

METHODS

In this study, we analyzed the composition of epidote from 27 hydrothermally altered intrusive rock samples from the three porphyry deposits (Gibraltar, Mount Polley, and Woodjam) and 12 rocks from the Nicola Group (Table 1). Intrusive and Nicola Group rock sample locations are shown in Figure 3 and listed in Appendix A. Two Nicola Group rock sample locations fall outside the extent of the maps in Figure 3. Volcanic and volcaniclastic rock samples from the Nicola Group were collected distal (>9 km) to porphyry mineralization, except for one sample collected near Woodjam (<1 km from mineralization; Fig. 3). Thick (75 µm) polished thin sections were prepared from the rock samples. Epidote grains were picked from heavy mineral separates (0.25–0.5 mm, >3.2 SG, and 0.8–1.0 A) of 25 subglacial till samples collected at locations within the epidote dispersal trains (down-ice) and up-ice from or distal to the alteration zones at each site (Fig. 3). Grains were mounted in epoxy and polished to expose their core.

Polished thin sections and grain mounts were examined with a TESCAN Mira3 field emission scanning electron microscope (SEM) at the Geological Survey of Canada (Ottawa, Ontario). Backscattered electron images were captured using a working distance of 15 mm, accelerating voltage of 20 kV, and probe current of 0.4 to 1 nA. Epidote composition analyses (Fe and Al) were performed using the Oxford Instruments energy dispersive spectrometry (EDS) system, which includes an X-MAX 80 silicon drift detector and Aztec 4.1 microanalysis software. Analyses were performed using an acquisition time of 3 s. The standard deviation of EDS analyses is 0.1 weight per cent oxides.

Epidote was analyzed for 58 elements by LA-ICP-MS at the Geological Survey of Canada (Ottawa, Ontario). The LA-ICP-MS analyses were done using a Photon Machines Analyte G2 (193 nm laser, equipped with a dual-volume cell) connected to an Agilent 7700x ICP-MS. Laser conditions included a laser fluence of 5 J/cm2, spot size of 30 to 65 µm (dependent on the size of the epidote), and repetition of 10 Hz. Helium gas (approximately 1 L/min) carried the ablated aerosol to the ICP-MS. A SQUID signal smoothing device was used on the carrier gas line. Signals were acquired on the ICP-MS using a total mass cycle time of 456 ms and dwell times of 2 to 4 ms for major elements, 4 to 8 ms for most trace elements, and 12 to 16 ms for specific trace elements of interest (i.e. As, Ag). Total analytical time was 100 s including 40 s of background measurement (laser off) and 60 s of signal analysis (laser on). The United States Geological Survey GSE-1G was used as the primary calibration standard and was analyzed twice every hour to correct for instrument drift. Once per hour, secondary standards NIST 612, GSD-1G, BCR-2G, and Po689 were analyzed to assess accuracy, with most elements falling within 5 to 10% of their reference values. Reference values for GSD-1G (Guillong et al., 2005), BCR-2G and GSE-1G (Jochum et al., 2005b), and NIST-612 (Kane, 1998) are based on preferred values from GeoReM (Jochum et al., 2005a). Reference values for Po689 (*see* Sylvester et al. (2005) for information about the Po series) were provided by Louis Cabri – CANMET (L. Cabri, pers. comm., 2020) and have been cross-referenced against other S-, As-, Ag-, and Au-bearing reference materials in the laboratory.

Analytical spectra were manually processed in GLITTER (Griffin et al., 2008), keeping only a 'clean' (i.e. inclusion-free) portion of each spectrum for data processing. Other mineral phases present as inclusions that were ablated during the analysis, such as Ti, P, or S peaks related to the potential presence of titanite, phosphate, or sulfide, respectively, were identified and excluded from the signals during processing. Trace-element concentrations were calibrated using Ca as an internal standard, determined on a JEOL8230 electron microprobe equipped with five wavelength spectrometers at the University of Ottawa. Operating conditions were 20 kV accelerating voltage, 20 nA beam current, and 5 µm spot size. Count times were 10 s on peak and 5 s on the

Table 1. Number of valid laser-ablation inductively coupled plasma mass spectrometry analyses of epidote in samples collected from porphyry mineralization and one regional rock type at study sites in the Quesnel terrane, British Columbia

Rock type	Site	Number of rock samples	Number of epidote analyses from rock samples	Number of till samples	Number of epidote grain analyses from till samples
Takomkane Batholith	Woodjam	7	69	7	60
Mount Polley Intrusive Complex	Mount Polley	10	81	9	81
Granite Mountain Batholith	Gibraltar	10	38	9	80
Nicola Group	Regional rock type	12	62	N/A	N/A

background to either side of the peak. Calibration standards were a mix of natural and synthetic minerals. Raw data were processed with the CITZAF program (Armstrong, 1988).

Further filtering of LA-ICP-MS analytical results to remove mineral phases other than epidote was based on major-element chemistry. Using the same classification scheme as Plouffe et al. (2019), analyses with greater than 42 weight per cent SiO2, greater than 0.5 weight per cent TiO_2, less than 15 weight per cent Al_2O_3, greater than 16 weight per cent Fe_2O_3, greater than 0.5 weight per cent MgO, greater than 24 weight per cent CaO, greater than 0.5 weight per cent Na_2O, greater than 0.25 weight per cent K_2O, and greater than 0.5 weight per cent P_2O_5 were classified as non-epidote and rejected from the interpreted data set. The result was 250 valid analyses of epidote in rock samples and 221 analyses of epidote grains from till with a rejection percentage of 25% (Table 1; Appendix A). In comparison, Pacey et al. (2020) report 41% rejection of their LA-ICP-MS epidote analyses. Analyses of P, Se, Te, and Pt were deemed to be semi-quantitative due to the absence of certified values in GSE-1G and/or the secondary standards (so that in house values were used for quantification), and although these elements are reported in Appendix A (indicated by '*' and italicized), the data have only been used in the principal component analysis (PCA) to assess relative interelement relationships.

Mean detection limits for LA-ICP-MS analyses are provided in Appendix A and represent the average of all values in the filtered data that fell below the minimum detection limit (i.e. all values with '<' symbols). Table 2 presents the minimum detection limits for the elements reported in this study.

A suite of 57 elements (i.e. variables), as determined by LA-ICP-MS, was used for PCA using the 'rgr' package (Garrett, 2013) within the R statistical software environment (R Core Team, 2018). To avoid the 'closure problem' inherent to compositional data, and prior to performing PCA, the data were transformed using the centred-log ratio transformation (Aitchison, 1986; Thió-Henestrosa and Martín-Fernández, 2005).

RESULTS

Plouffe et al. (2019) recognize three general forms of epidote in the rock samples:

- Euhedral and poikilitic epidote that replaces feldspar or overprinting chlorite is typical of the metamorphosed Nicola Group rocks (Fig. 4a). Some of this epidote is less than 0.25 mm; therefore, it would not be recovered in the 0.25 to 0.5 mm size fraction of till samples.
- Epidote that replaces chlorite pseudomorphs after biotite with a layered and, in places, deformed wavy texture and titanite inclusions is interpreted to be hydrothermal in origin. It is also found in close association with undeformed epidote (Fig. 4b).
- The dark to pale pistachio-green epidote that occurs in veins or in association with chlorite, quartz, and sulfides is interpreted as hydrothermal in origin. This form of epidote has a pitted texture due to abundant mineral inclusions common in hydrothermal minerals. In backscattered electron images, this epidote shows complex crystal growth patterns (Fig. 4c).

The SEM study of epidote revealed variable textures. Backscattered electron images showed mottled to zoned textures attributed to variation in Fe and Al content. For example, based on EDS analyses and assuming total Fe oxides are Fe_2O_3, the darker shades of grey in the epidote samples presented in Figure 4 contain 10.4 to 14.7 weight per cent Fe_2O_3 and 23.1 to 26.6 weight per cent Al_2O_3, and the lighter shades of grey are areas that contain 14.3 to 16 weight per cent Fe_2O_3 and 22.0 to 23.3 weight per cent Al_2O_3. Similar zonation and associated variable Fe and Al content was reported by Cooke et al. (2014) in epidote resulting from hydrothermal alteration in porphyry copper mineralization. With a laser spot size of 30 to 65 µm, we could not avoid the Fe-Al zoning in epidote. Complex crystal growth patterns, as those observed in epidote veins, appear to be a unique characteristic of hydrothermal epidote (Fig. 4c). The same texture was observed in some epidote grains recovered from till (Fig. 4d). In addition to these textures, we observed

Table 2. Mean minimum detection limits (MDL) for reported elements

Element	Mean MDL (ppm)
Sc	0.69
Cr	3.33
Cu	0.13
As	0.09
Y	0.01
Sb	0.38
La	0.01
Ce	0.05
Pr	0.01
Nd	0.07
Sm	1.16
Eu	0.03
Gd	0.56
Tb	0.01
Dy	0.18
Ho	0.02
Er	0.33
Tm	0.08
Yb	0.4
Lu	0.48
Hf	0.59
Th	0.08

a number of mineral inclusions, including titanite, rutile, hematite, and apatite, under the SEM in epidote samples from all rock types. Chalcopyrite inclusions were observed in epidote and allanite in some samples from Gibraltar (see also Kobylinski et al., 2017).

Laser-ablation inductively coupled plasma mass spectrometry analyses of epidote from the various rock types show important differences in the average concentrations of certain elements (Table 3); these geochemical differences have the potential to indicate the source of detrital epidote. The average As and Sb concentrations in epidote vary among the rock types, with no apparent consistent pattern between intrusive and Nicola Group rocks. On the other hand, Y, total REE (ΣREE), Sc, Th, Hf, and Cr occur, on average, in higher concentrations in Nicola Group epidote compared to epidote from intrusive rocks. Using these elements, we present three correlation graphs that could serve to differentiate the source of detrital epidote based on its composition: As versus Sb (Fig. 5), ΣREE versus Y (Fig. 6), and Sc+Cr+Y versus Th+Hf (Fig. 7).

In the As versus Sb correlation graph (Fig. 5), epidote from the Mount Polley Intrusive Complex and the Takomkane batholith (Woodjam) generally plots with higher As (approximately >10 ppm) and Sb (approximately >4 ppm) concentrations than epidote from the Nicola Group rocks (Fig. 5a, b). The notable exceptions are a number of Nicola Group epidotes with greater than 10 ppm As or greater than 4 ppm Sb, shown in a darker green in Figure 5. All of these epidotes are from rock samples located near (<1 km) porphyry mineralization or intrusive rocks hosting the mineralization (see their locations in Fig. 3). The compositions of epidote grains from till at Mount Polley and Woodjam overlap in large part with epidotes from intrusive rocks. No distinction exists between the composition of epidote grains in till in down-ice versus up-ice or distal samples (Fig. 5a, b). Epidote from the Granite Mountain batholith (Gibraltar) generally contains As and Sb in concentrations similar to Nicola Group epidote (Fig. 5c); however, a few epidotes from the Granite Mountain batholith do contain greater than 4 ppm Sb. For comparison, the metamorphic (M) and porphyry (P) epidote fields defined by Wilkinson et al. (2017b) are shown in Figure 5 and discussed below.

Two additional simple correlation graphs accentuate the chemical differences between epidote from Nicola Group rocks and epidote from intrusive rocks. Plots of Y versus ΣREE, corresponding to the total of La to Lu (Appendix A) show that, for the same ΣREE concentration, Y concentrations are generally lower in epidote from the Mount Polley Intrusive Complex compared to Nicola Group epidote (Fig. 6a). At Woodjam, most epidote from the Takomkane batholith contains less than 19 ppm Y and between 10 and 100 ppm ΣREE in contrast to Nicola Group epidote, which generally contains greater than 19 ppm Y and 10 to 6900 ppm ΣREE (Fig. 6b). At Gibraltar, epidote in the Granite Mountain batholith generally has lower Y and ΣREE concentrations than in Nicola Group epidote, but there is a strong overlap between populations (Fig. 6c). At all sites, there is a strong overlap between the composition of epidote in till and epidote from intrusive rocks, irrespective of whether the till samples were collected within the epidote dispersal train (down-ice) or outside of it (distal and up-ice) (Fig. 3, 6).

A plot of Sc+Cr+Y versus Th+Hf provides additional support to discriminate between intrusive and Nicola Group epidotes (Fig. 7). These elements were grouped based on their general concentration ranges: 0.01 to 10 ppm for Th and Hf, and 10 to 1000 ppm for Sc, Cr, and Y. Most of the epidote in intrusive rocks at the three sites contains 0.01 to 6 ppm Hf+Th and 5 to 100 ppm Sc+Cr+Y, as opposed to Nicola Group epidote, which generally contains 0.1 to 10 ppm Hf+Th and 35 to 1600 ppm Sc+Cr+Y. As with the ΣREE versus Y correlation, there is an overlap between the epidote from intrusive and Nicola Group rocks, and most of the epidote in till mimics the composition of epidote from intrusive rocks, with no distinction between the down-ice and up-ice or distal samples (Fig. 7).

Principal component analysis was performed to differentiate the two main populations of epidote based on the entire LA-ICP-MS geochemical data set. The first four principal components (PC1, PC2, PC3, and PC4) correspond to the

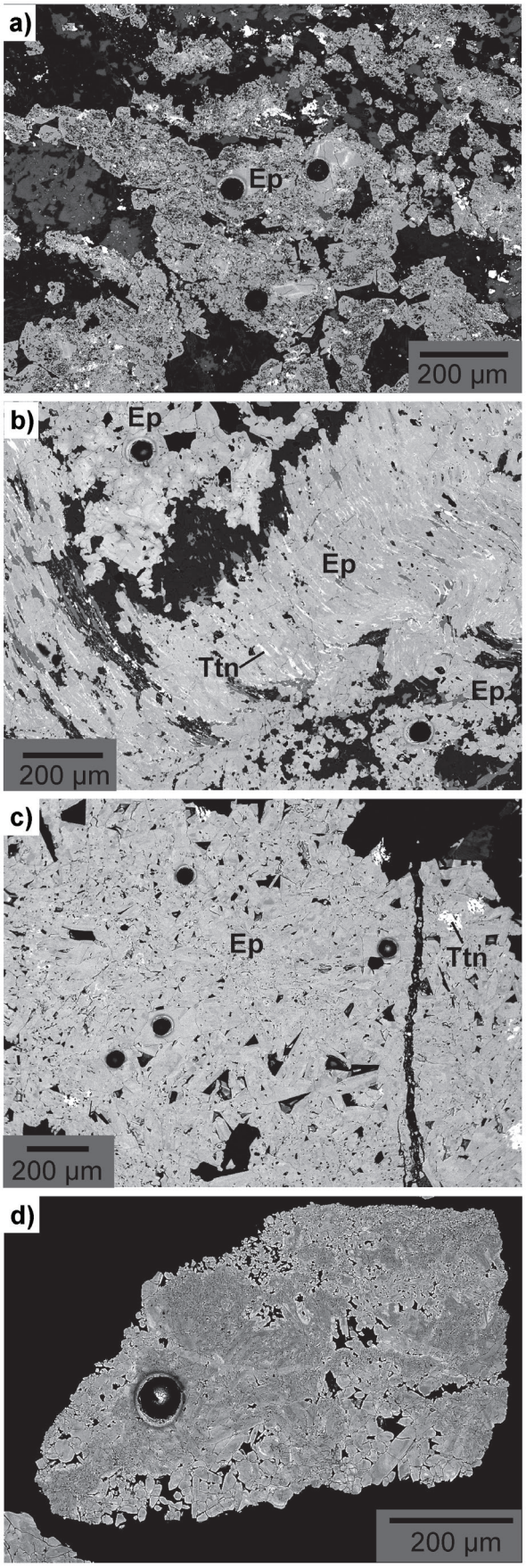

Figure 4. Backscattered electron images of epidote (Ep): **a)** non-homogeneous poikilitic metamorphic epidote with abundant iron-titanium oxide (white specks) in a sample (14PSC357) of Nicola Group rock; **b)** hydrothermal epidote replacing chlorite pseudomorph after biotite with a wavy texture and titanite (Ttn) inclusions, in close association with undeformed epidote (top left), in a sample (73Q202) of the Granite Mountain batholith; **c)** hydrothermal epidote with complex crystal growth patterns in an intrusive rock sample (13CDBWJ05) from the Woodjam prospect; **d)** complex crystal growth patterns in an epidote grain recovered from till (sample 11PMA012) at the Woodjam prospect. Note the 50 µm circular laser ablation pits visible in all images.

Table 3. Average concentration (ppm) of selected elements in epidote in samples collected from porphyry mineralization and one regional rock type at study sites in the Quesnel terrane, British Columbia

Rock type	Site	As	Sb	Y	ΣREE	Sc	Th	Hf	Cr
Takomkane batholith	Woodjam	55	93	13	58	10	0.5	0.6	3*
Mount Polley Intrusive Complex	Mount Polley	38	7	35	416	7	0.4	0.4*	1*
Granite Mountain batholith	Gibraltar	3	6	28	99	57	0.6	0.3*	6
Nicola Group	Regional rock type	25	17	82	552	172	5	1	57
* – below the mean detection limit									

linear combinations of selected elements that account for most of the data variability (55%). For simplicity, the data set variance is displayed in terms of PC1 (24%) and PC2 (16%), which are plotted in Figure 8. Rare-earth elements yield high positive PC1; PC2 is negative for light REE (La, Ce, Pr, Nd, Sm, Eu, Gd), and positive for heavy REE (Tb, Dy, Ho, Er, Tm, Y, Lu). High positive PC2 is observed for Na, Mn, Mg, K, Rb, Cr, and Sc, and Co, Ni, and Zn have overall negative PC1 and PC2 loadings (Fig. 8). Other elements, such as Ga, Fe, and Sr, yield high negative PC2 loadings. Epidotes in intrusive rocks from the Mount Polley, Gibraltar, and Woodjam deposits are roughly distinguished in terms of their PC2 scores (Woodjam>Gibraltar>Mount Polley). Epidote of the Mount Polley Intrusive Complex yields the lowest PC2 scores given its high concentrations of Ga, Ge, Fe, and Sr (Fig. 8a). With high Na, K, Mn, Cr, Th, and Sc concentrations, epidote from the Takomkane batholith at Woodjam yields the highest PC2 scores (Fig. 8b). Epidote in Nicola Group rocks is generally characterized by positive PC1 and PC2 scores, with some exceptions. Nicola Group epidotes with high As or Sb concentrations (identified in Fig. 5), are shown by dark green triangle in Figure 8 and are mostly characterized by a high PC1 score related to high ΣREE content. At Woodjam and Gibraltar, the composition of epidote from intrusive rocks, Nicola Group rocks, and till largely overlap in PC space (Fig. 8b, c). Conversely, at Mount Polley, the till and Nicola Group epidotes are strongly decoupled from epidote in intrusive rocks with respect to their PC2 scores (Fig. 8a).

DISCUSSION

Interpretation of epidote chemistry as a means for detecting hydrothermal alteration associated with porphyry copper mineralization must account for: 1) factors that control epidote composition and 2) the variability of epidote composition in porphyry systems as reported in other studies. Epidote composition is controlled by the primary mineral it replaced, the host rock, hydrothermal fluid composition, temperature, and, to a lesser extent, pressure (Bird and Helgeson, 1980; Arnason et al., 1993; Bird and Spieler, 2004; Pacey et al., 2020). Also, co-forming minerals such as sulfides do affect the composition of epidote in a porphyry system. For instance, within the pyrite-rich phyllic alteration halo of the Black Mountain and Nugget Hill porphyry copper deposits in the Philippines, epidote is depleted in As, Sb, and Pb because these elements are dominantly incorporated by pyrite (Cooke et al., 2014). Outside the pyrite halo and within the propylitic alteration zone, these same elements substitute into epidote (Cooke et al., 2014).

In addition to Cooke et al. (2014), other studies have illustrated the variability in the composition of epidote within a single porphyry copper deposit. At the Bingham deposit in Utah, U.S.A., the MnO content of vein epidote increases from 0.08 weight per cent in the centre of the deposit to 0.73 weight per cent 1.1 km from mineralization (Bowman et al., 1987). At the Tintic deposit, 70 km south of the Bingham deposit, Mn in epidote decreases over a distance of approximately 1 km, from a maximum of 1.18 weight per cent MnO in the actinolite subzone to 0.15 weight per cent MnO in the outer chlorite subzone (Norman et al., 1991). At the Mount Milligan deposit in central British Columbia, along three transects, the Fe content of epidote, expressed as the pistachite ratio ($PS = Fe^{3+} / Fe^{3+} + Al^{3+}$), decreases over 200 to

Figure 5. Correlation plots of As versus Sb concentrations in epidote from Nicola Group rocks, intrusive rocks, and grains recovered from till from the **a)** Mount Polley, **b)** Woodjam, and **c)** Gibraltar occurrences in south-central British Columbia. Up-ice and distal sample (dark blue crosses) numbers are indicated in the legends and their locations are shown in Figure 3. Note that the same Nicola Group epidote data are presented in all three graphs. Grey dashed and dotted lines define the range of As and Sb concentrations in metamorphic (M) and porphyry (P) epidote determined by Wilkinson et al. (2017b). Horizontal and vertical dashed lines represent the mean minimum detection limit (MDL) for each element. Concentrations below the detection limit are plotted using data not filtered for MDL.

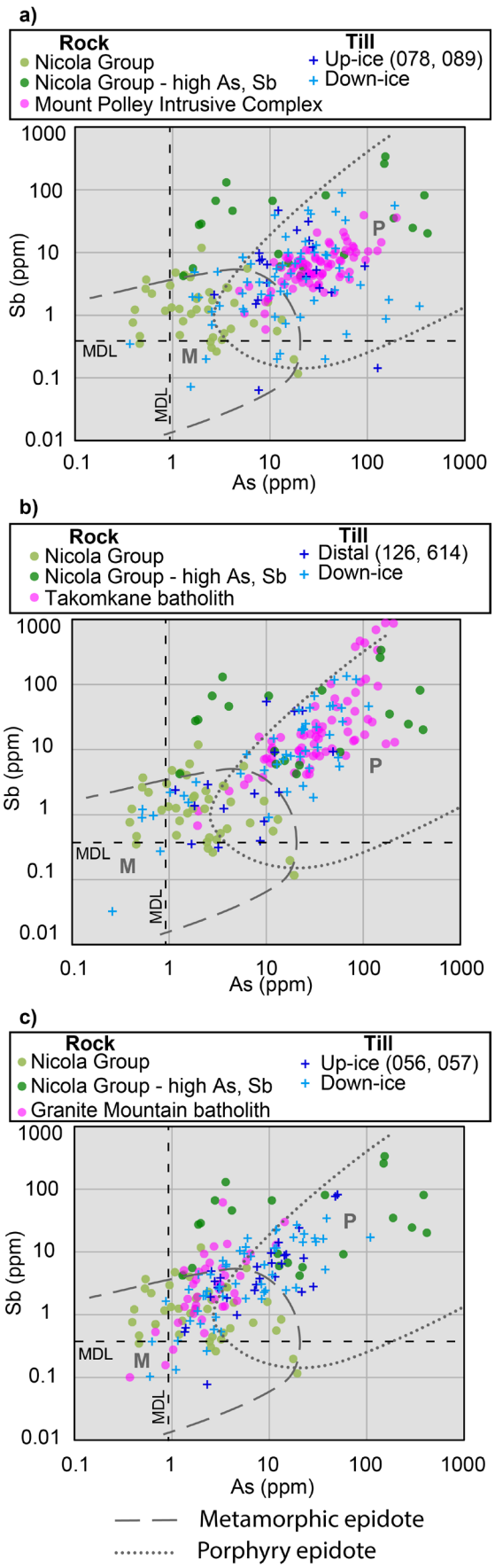

400 m distances, from median values of PS30 and PS36 near the potassic zone to PS25 and PS26 in the outer propylitic zone (Jago et al., 2014). At this same site and in parallel to these trends, epidote trace-element chemistry shows a lateral increase in V, Mn, Sb, Zr, and As, and a lateral decrease in Pb, Cu, Au, and Mo, with increased distance from the potassic zone (Jago et al., 2014). At the El Teniente deposit in Chile, epidote composition follows a pattern similar to that observed by Cook et al. (2014) in the Philippines, having a broad proximal zone of low As in epidote and reaching higher values approximately 3 km from the edge of the ore shell (Wilkinson et al., 2017a). Using gridded values, Wilkinson et al. (2017a) show high concentrations of La, Zr, Zn, Yb, and Y in epidote defining a broad halo around the El Teniente deposit. At the E48 and E26 porphyry Cu-Au deposits in Australia, Pacey et al. (2020) report on the composition of epidote which shows a lateral increase in Ti, As, Sb, and V, and a lateral decrease in Ba towards the deposits. These studies illustrate a wide range of elemental substitutions that can take place in epidote and the variability in epidote composition within a single porphyry system.

Despite this variability in epidote composition within a single porphyry system, Wilkinson et al. (2017b) suggest that porphyry-related epidote is enriched in elements carried by porphyry hydrothermal fluids such as As and Sb, which, in contrast, are at low concentrations in metamorphic epidote. Wilkinson et al. (2017b) reached this conclusion following the analysis of epidote from three porphyry Cu-Au and Cu-Mo systems (Resolution (United States), El Teniente (Chile), Baguio (Philippines)) that contained greater than 4 ppm As and greater than 0.2 ppm Sb, in contrast with epidote from metamorphic rocks of the Dalradian and Moine supergroups in Scotland, which generally yielded less than 20 ppm As and less than 6 ppm Sb (Fig. 5; Wilkinson et al., 2017b, Fig. 3). Wilkinson et al. (2017b) compared metamorphic and porphyry-related epidote from widely separated geological environments. Despite this limitation, the As versus Sb correlation graph of Wilkinson et al. (2017b) provides good indications of the source (metamorphic or porphyry related) of the epidote. The greater abundance of As and Sb in porphyry-related epidote compared to metamorphic epidote is certainly not encountered in all geological environments because the reverse relationship was observed by Pacey et al. (2020). Because of this variability in epidote chemistry, we tested the utility of As and Sb as discriminators of porphyry-related and metamorphic epidote.

The concentrations of As and Sb in epidote from Nicola Group rocks generally fall within the metamorphic field of Wilkinson et al. (2017b), with notable exceptions having greater than 10 ppm As or greater than 4 ppm Sb (dark green in Fig. 5). As indicated above, these epidotes are from one rock sample located less than 1 km from one of the mineralized zones at Woodjam and three rock samples located greater than 9 km from Gibraltar ore but near (less than 1 km) the Granite Mountain batholith, which hosts the mineralization (see Nicola Group samples marked with an asterisk in Fig. 3). Some of these epidotes with high As or

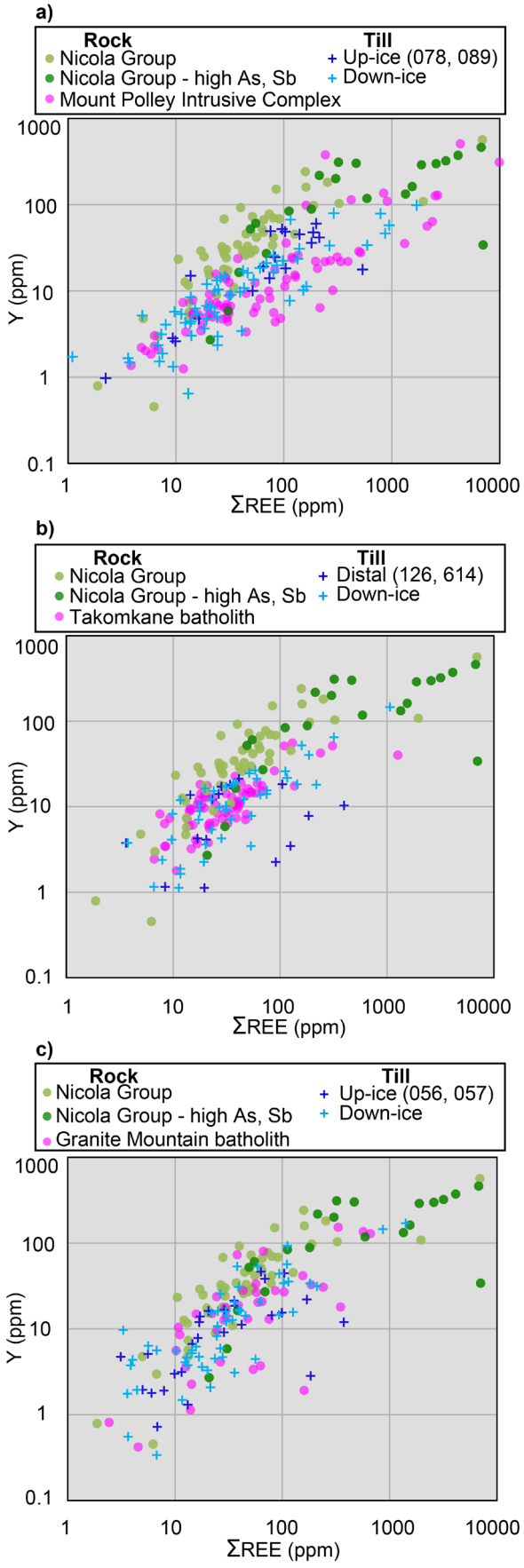

Figure 6. Correlation plots of total rare-earth element (ΣREE) versus Y concentrations in epidote from Nicola Group rocks, intrusive rocks, and grains recovered from till from the **a)** Mount Polley, **b)** Woodjam, and **c)** Gibraltar occurrences in south-central British Columbia. Up-ice and distal sample (dark blue crosses) numbers are indicated in the legends and their locations are shown in Figure 3. Note that the same Nicola Group epidote data are presented in all three graphs.

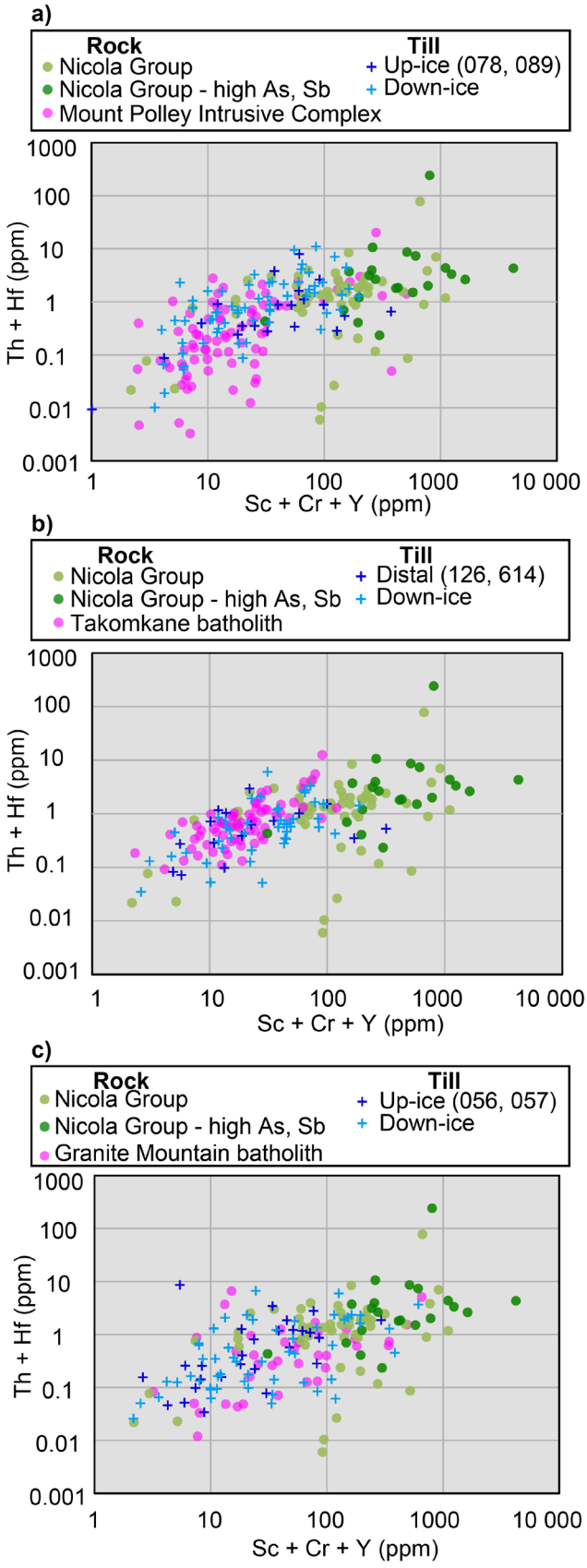

Figure 7. Correlation plots of Sc+Cr+Y versus Th+Hf concentrations in epidote from Nicola Group rocks, intrusive rocks, and grains recovered from till from the **a**) Mount Polley, **b)** Woodjam and, **c)** Gibraltar occurrences in south-central British Columbia. Up-ice and distal sample (dark blue crosses) numbers are indicated in the legends and their locations are shown in Figure 3. Note that the same Nicola Group epidote data are presented in all three graphs.

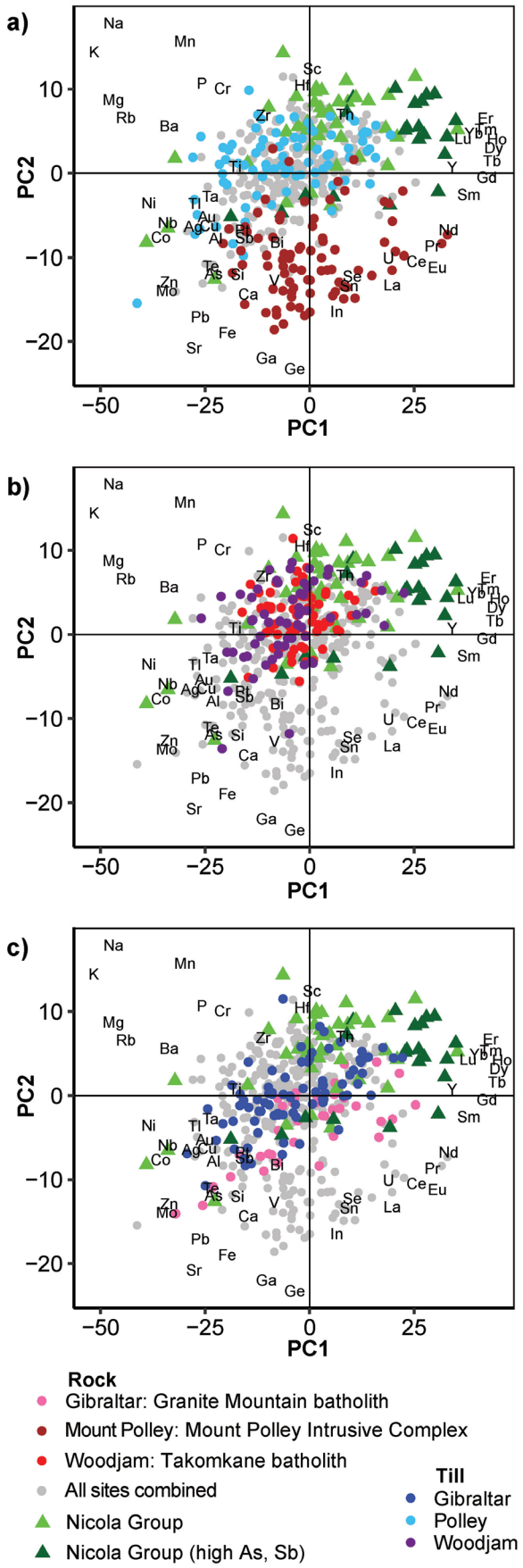

Figure 8. Principal component analysis PC1–PC2 score biplots showing the chemical variation of epidote from mineralized intrusions, Nicola Group volcanic rocks (metamorphic), and till samples collected at the **a)** Mount Polley, **b)** Woodjam, and **c)** Gibraltar occurrences in south-central British Columbia.

Sb levels occur in veins. Building on the observations of Wilkinson et al. (2017b), we interpret epidote occurring in veins within Nicola Group rocks and having greater than 10 ppm As or greater than 4 ppm Sb to be hydrothermal in origin and related to the porphyry mineralization.

Epidote in the intrusive rocks at Mount Polley and Woodjam dominantly fall within the porphyry field, defined by Wilkinson et al. (2017b) as having much greater than 4 ppm As and much greater than 0.6 ppm Sb, suggesting an hydrothermal origin (Fig. 5a, b). In contrast, epidotes at Gibraltar contain concentrations of As and Sb that dominantly fall within the metamorphic field (Wilkinson et al., 2017b) (Fig. 5c). A few epidotes at Gibraltar have greater than 8 ppm Sb and fall outside of both fields (Fig. 5c). It appears that syn- and post-mineralization deformation and associated greenschist metamorphism at Gibraltar (which is a higher metamorphic grade than the two other sites; Greenwood et al., 1991; Read et al., 1991; Panteleyev et al., 1996) has affected the As and Sb content of hydrothermal epidote, or has produced metamorphic epidote with lower As levels; consequently, in a porphyry copper system metamorphosed to greenschist facies, the As and Sb concentrations in epidote might not be a reliable identifier of a hydrothermal versus metamorphic origin.

On the As versus Sb correlation graph (Fig. 5), epidote grains from till at Mount Polley and Woodjam dominantly fall in the porphyry field, with fewer grains within the metamorphic field (Fig. 5a, b), suggesting a predominance of porphyry-related epidote in till (>>4 ppm As and >>0.6 ppm Sb) with only a minor proportion derived from the metamorphosed Nicola Group volcanic rocks. At Gibraltar, epidote grains from till fall within the metamorphic and porphyry fields (Fig. 5c).

Our results indicate that no clear distinction exists between epidote in till collected down-ice, up-ice, or distally from mineralization at each study site (Fig. 5). The presence of porphyry-related epidote with much greater than 4 ppm As and much greater than 0.6 ppm Sb in till samples collected up-ice from the main epidote dispersal train at Gibraltar and Mount Polley might be due to one or a combination of two factors: 1) hydrothermal alteration directly related to these deposits might be more extensive than previously thought and might extend into the up-ice region and/or 2) an unknown source of porphyry mineralization with associated alteration might be present in the up-ice region. At Woodjam, five porphyry-related epidote grains from two till samples (sites 126 and 614; Fig. 3b, 5b) were obtained down-ice and outside of the epidote dispersal train, where the local bedrock (Neogene Chilcotin basalt) is not a source of epidote (Plouffe et al., 2016). We interpret this to represent either 1) glacial transport of porphyry-derived epidote grains 10 km from their source or 2), again, hydrothermal alteration associated with an undiscovered source of porphyry mineralization and alteration in subcropping rock units of this region.

The correlation plots of ΣREE versus Y and Sc+Cr+Y versus Hf+Th do not discriminate between porphyry related (high As and Sb) and metamorphic Nicola Group epidotes (Fig. 6, 7); rather, they discriminate between epidotes from granitoids versus mafic Nicola Group volcanic rock sources. The ΣREE and Y content of granitoids varies from site to site (Fig. 6); however, values of less than 100 ppm Sc+Cr+Y and less than 6 ppm Hf+Th typically reflect a granitoid provenance (Fig. 7). We suspect that the controlling factor of this suite of elements in epidote is in part that the primary mineral composition replaced by epidote is different in felsic (granitoids) and mafic (Nicola Group) rocks. The significant overlap between epidote grains derived from till and epidotes from intrusive rock at the three study sites is observed on these correlation graphs (Fig. 6, 7), and suggests that most of the epidote in till is derived from granitoids.

We interpret the PCA to indicate that epidote composition is the result of multiple geological factors and processes (primary mineral it replaced, the host rock, hydrothermal fluid composition, temperature, and pressure), so that the first four principal components only account for 55% of the total variance. The application of PCA to differentiate the source of epidote in our study is probably further complicated by the fact that magma and fluid sources of the Nicola Group volcanic rocks and the coeval porphyry plutons are similar because both are part of the same magmatic arc; consequently, using the full suite of elements potentially introduces variability into the interpretation of epidote composition that obscures the two-group distinction of epidote attempted here. As a result, PCA alone is insufficient to accurately distinguish between intrusive- and metamorphic-related geochemical subgroups of epidote. Further application of unsupervised machine-learning techniques (e.g. cluster and linear discriminant analysis), potentially using a smaller suite of elements, combined with detailed petrographic studies may provide better results.

It might also be possible to assess porphyry fertility based on epidote composition (Cooke et al., 2014). In their summary of epidote composition of the Baguio porphyry district in the Philippines, Cooke et al. (2014) show that epidote within the pyrite halo of a fertile porphyry system have elevated median concentrations of Cu (11–28 ppm), which they suggest is a potential fertility indicator (Cooke et al., 2014, Fig. 15). At Mount Milligan, 325 km north of Gibraltar, the highest Cu concentration in epidote near porphyry mineralization is 45 ppm (Jago et al., 2014). In contrast, Pacey et al. (2020) detected Cu in only 9% of their LA-ICP-MS epidote analyses, with a maximum concentration of 5 ppm. In our study, some epidotes from the intrusive rocks and till at Gibraltar and Mount Polley have Cu concentrations that exceed the highest median values of ore zone epidote at the Baguio district (Cooke et al., 2014) and Mount Milligan (Fig. 9). In comparison, the mean Cu concentration in epidote from Nicola Group rocks (5 ppm) is lower than at the Granite Mountain batholith (37 ppm) and the Mount Polley Intrusive Complex (207 ppm; Fig. 9). Three of the highest Cu concentrations in epidote (26, 30, and 42 ppm) occur

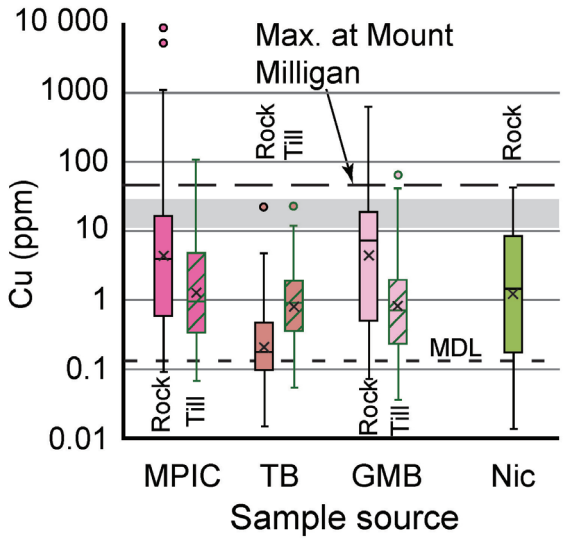

Figure 9. Box and whisker plot showing quartile distribution of Cu concentrations in epidote from rocks and till at the Gibraltar (Granite Mountain batholith (GMB)), Mount Polley (Mount Polley Intrusive Complex (MPIC)), and Woodjam (Takomkane batholith (TB)) occurrences in south-central British Columbia. Concentrations of Cu in epidote in Nicola Group rocks (Nic) are also shown for comparison. The × denotes mean concentration. The grey zone represents the highest Cu median concentrations observed in epidote in rocks collected less than 1 km from porphyry mineralization in the central Baguio district, Philippines (11–28 ppm Cu; Cooke et al., 2014). The upper dashed line shows the maximum concentration observed in epidote at Mount Milligan, British Columbia (Jago et al., 2014). The lower dashed line is the minimum detection limit (MDL); concentrations below the detection limit are plotted using data not filtered for MDL.

in a sample from the Nicola Group rocks with elevated As and Sb values, located less than 1 km northeast of the Granite Mountain batholith, further suggesting that this epidote could be of hydrothermal origin and related to the porphyry copper mineralization. The absence of epidote with high Cu concentration at Woodjam could be related to the position of the shallow hydrothermal alteration zone sampled in our study relative to the main zone of mineralization; the shallow hydrothermal alteration at Woodjam might be in a zone where epidote has low Cu concentrations. Based on the Cu concentrations measured in our samples and those reported by Cooke et al. (2014) and Jago et al. (2014), we suggest that concentrations of greater than 30 ppm Cu in epidote can provide an indication of fertility and are significant from a mineral exploration point of view; moreover, we recognize that more tests on epidote from barren and mineralized intrusions are necessary to assess the robustness of using Cu content in epidote as a fertility indicator. Finally, the form of copper in epidote is still unknown; it could substitute in the epidote crystal lattice or occur as nanoparticles (cf. Cooke et al., 2014).

Results from this study have important implications for mineral exploration. In a favourable geological setting for porphyry mineralization, such as in regions underlain by Late Triassic to Early Jurassic felsic to intermediate intrusions of the Quesnel terrane, greater abundance of epidote in heavy mineral concentrates (HMC) of till compared to regions underlain by Nicola Group rocks can provide a first indication of a porphyry hydrothermal system associated with an intrusion, even in the absence of sought metals (e.g. copper, molybdenum, gold) and indicator minerals (e.g. chalcopyrite, gold grains; Fig. 1b, 3). The texture of epidote grains recovered from detrital sediments with complex crystal growth forms is an apparent indicator of hydrothermal origin (Fig. 4c, d). The chemical composition of detrital epidote grains can provide an indication of their source: granitoids epidote typically contain less than 6 ppm Hf+Th and less than 100 ppm Sc+Cr+Y (Fig. 7), and porphyry-related epidotes much greater than 4 ppm As and much greater than 0.6 ppm Sb (Fig. 5). Lastly, the copper content of epidote (approximately >30 ppm Cu) might provide an indication of copper fertility (Fig. 9); however, given the overlap in epidote data from granitoid rocks versus mafic volcanic rocks (Fig. 6, 7) and from hydrothermal versus metamorphic settings (Fig. 5), and the presence of a Cu fertility signal in only a few detrital grains, we do not recommend a grain-by-grain characterization as was applied, for example, by Mao et al. (2017) to apatite recovered from till in British Columbia. Instead, we suggest that detrital epidote provenance should be established from compositional data using a large population of detrital epidote grains. In our study, LA-ICP-MS analyses of 60 to 81 epidote grains from seven to nine till samples at each study site (Table 1) was sufficient to identify porphyry-related epidote within regional dispersal trains (Fig. 3).

Determining the abundance of epidote in till (Fig. 3), along with its chemical composition, could become a routine exploration method in the search for porphyry copper mineralization buried under glacial sediments in the Canadian Cordillera. Given the size of the studied epidote anomalies in till which reach approximately 19 km^2 at Woodjam, 21 km^2 at Polley, and 135 km^2 at Gibraltar (Fig. 3), a till sample spacing of 2 km (one sample per 4 km^2) would be sufficient to detect an epidote anomaly. This method could be efficient in a scenario where mineralization with metal enrichment is at depth and only the propylitic alteration zone is exposed to glacial erosion.

In addition to epidote, other porphyry copper indicator minerals could be identified in till or other detrital sediments (Plouffe and Ferbey, 2017; Beckett-Brown et al., 2019, this volume; McClenaghan et al., this volume). Of course, the identification of ore minerals (e.g. chalcopyrite) in till represents additional evidence of porphyry copper mineralization in the source region of glaciers. Focusing on the objective of our research — the detection of buried porphyry systems

with no mineralization exposed to glacial erosion — the REE composition of zircon in till (e.g. Ce/Nd) can provide complementary information about the potential of an intrusion to host porphyry mineralization (Ballard et al., 2002; Liang et al., 2006; Dilles et al., 2015; Shen et al., 2015). For instance, in a study at Gibraltar, out of 45 zircon grains recovered from five till samples, only one sample, located close (<1 km) to mineralization, contained zircon with a Ce/Nd ratio greater than 20, which is indicative of oxidizing magmatic conditions favourable for porphyry mineralization (Plouffe et al., 2018, 2019).

CONCLUSION

Our study shows that hydrothermally derived epidote recovered from till can be used for porphyry copper mineral exploration. Its greater abundance in till heavy mineral concentrates near porphyry mineralization along with its composition can be indicative of a porphyry copper source. Epidotes with less than 6 ppm Hf+Th and less than 100 ppm Sc+Cr+Y are typically derived from granitoid rocks. Epidotes with much greater than 4 ppm As and much greater than 0.6 ppm Sb are representative of a hydrothermal alteration zone associated with porphyry mineralization. Concentrations greater than 30 ppm Cu in epidote recovered from till can provide an estimate of the fertility potential of the bedrock source. Epidote as an indicator mineral of porphyry copper mineralization is likely to be widely applicable because it is common in propylitic alteration of porphyry systems.

We have used epidote chemistry to differentiate two broad geological sources of epidote in till within a specific geological setting prospective for porphyry copper mineralization: the Quesnel terrane of south-central British Columbia. The application of epidote as an indicator mineral in mineralizing environments other than porphyry systems remains unexplored. The epidote method tested here for till should be applicable to stream sediment settings, given the resistant nature of this mineral; however, its applicability to epidote obtained from streams or other detrital sediments in unglaciated landscapes with thick regolith requires further testing. Future work should also explore the application of unsupervised machine-learning techniques to characterize epidote genesis and provenance.

ACKNOWLEDGMENTS

This research would not have been possible without the contribution of rock samples by a number of individuals, who took time to retrieve samples from their collection or, in some cases revisit field sites. These include J.B. Chapman, C.H. Kobylinski, C. Rees, and P. Schiarizza. C. Bjerklund, C. Hutton, G. Marquis, N. Rogers, and J. Tomkins from the TGI management team provided support to enable this activity. The manuscript benefited from review by N. Rogers and A. Rukhlov.

REFERENCES

Aitchison, J., 1986. The statistical analysis of compositional data; Monographs on statistics and applied probability; Chapman and Hall, London, 416 p.

Armbruster, T., Bonazzi, P., Akasaka, M., Bermanec, V., Chopin, C., Gieré, R., Heuss-Assbichler, S., Liebscher, A., Menchetti, S., Pan, Y., and Pasero, M., 2006. Recommended nomenclature of epidote-group minerals; European Journal of Mineralogy, v. 18, no. 5, p. 551–567. https://doi.org/10.1127/0935-1221/2006/0018-0551

Armstrong, J.T., 1988. Quantitative analysis of silicates and oxide minerals: comparison of Monte-Carlo, ZAF and Phi-Rho-Z procedures; *in* Microbeam Analysis, (ed.) D.E. Newbury; San Francisco Press, San Francisco, p. 239–246.

Arnason, J.G., Bird, D.K., and Lion, J.G., 1993. Variables controlling epidote composition in hydrothermal and low-pressure regional metamorphic rocks; 125 years Knappenwand –proceedings of a symposium, Salzburg, Austria, p. 17–25.

Ash, C.H., Rydman, M.O., Payne, C.W., and Panteleyev, A., 1999. Geological setting of the Gibraltar mine south central British Columbia (93B/8, 9); *in* Exploration and mining in British Columbia 1998, British Columbia Ministry of Energy and Mines, p. A1–A15.

Averill, S.A., 2011. Viable indicator minerals in surficial sediments for two major base metal deposit types: Ni-Cu-PGE and porphyry Cu; Geochemistry: Exploration, Environment, Analysis, v. 11, p. 279–291. https://doi.org/10.1144/1467-7873/10-IM-022

Ballard, J.R., Palin, J.M., and Campbell, I.H., 2002. Relative oxidation states of magmas inferred from Ce(IV)/Ce(III) in zircon: application to porphyry copper deposits of northern Chile; Contributions to Mineralogy and Petrology, v. 144, p. 347–364. https://doi.org/10.1007/s00410-002-0402-5

Beckett-Brown, C.E., McDonald, A.M., and McClenaghan, M.B., 2019. Unravelling tourmaline in mineralized porphyry systems: assessment as a valid indicator mineral; *in* Targeted Geoscience Initiative: 2018 report of activities, (ed.) N. Rogers; Geological Survey of Canada, Open File 8549, p. 345–351. https://doi.org/10.4095/313669

Berry, L.G., Mason, B., and Dietrich, R.V., 1983. Mineralogy; W.H. Freeman and Company, San Francisco, 561 p.

Bird, D.K. and Helgeson, H.C., 1980. Chemical interaction of aqueous solutions with epidote-feldspar mineral assemblages in geologic systems: 1. Thermodynamic analysis of phase relations in the system CaO-FeO-Fe_2O_3-Al_2O_3-SiO_2-H_2O-CO_2; American Journal of Science, v. 280, no. 9, p. 907–941. https://doi.org/10.2475/ajs.280.9.907

Bird, D.K. and Spieler, A.R., 2004. Epidote in geothermal systems; Reviews in Mineralogy and Geochemistry, v. 56, p. 235–300. https://doi.org/10.2138/gsrmg.56.1.235

Bowman, J.R., Parry, W.T., Kropp, W.P., and Kruer, S.A., 1987. Chemical and isotopic evolution of hydrothermal solutions at Bingham, Utah; Economic Geology, v. 82, no. 2, p. 395–428. https://doi.org/10.2113/gsecongeo.82.2.395

Bysouth, G.D., Campbell, K.V., Barker, G.E., and Gagnier, G.K., 1995. Tonalite-trondhjemite fractionation of peraluminous magma and the formation of syntectonic porphyry copper mineralization, Gibraltar mine, central British Columbia; *in* Porphyry deposits of the northwestern Cordillera of North America, (ed.) T.G. Schroeter; Canadian Institute of Mining, Metallurgy and Petroleum, Special Volume 46, p. 201–213.

Clarke, G., Northcote, B., Katay, F., and DeGrace, J.R., 2018. Exploration and mining in British Columbia, 2018: a summary; *in* Provincial overview of exploration and mining in British Columbia, 2018; British Columbia Ministry of Energy, Mines and Petroleum Resources, British Columbia Geological Survey, Information Circular 2019-01, p. 1–37.

Cooke, D.R., Baker, M., Hollings, P., Sweet, G., Zhaoshan, C., Danyushevsky, L., Gilbert, S., Zhou, T., White, N., Gemmell, J.B., and Inglis, S., 2014. New advances in detecting the distal geochemical footprints of porphyry systems – epidote mineral chemistry as a tool for vectoring and fertility assessments; *in* Building exploration capability for the 21st century, (ed.) K.D. Kelley and H.C. Golden; Society of Economic Geologists, Special Publication No. 18, p. 127–152.

del Real, I., Hart, C.J.R., Bouzari, F., Blackwell, J.L., Rainbow, A., Sherlock, R., and Skinner, T., 2013. Paragenesis and alteration of the Southeast Zone and Deerhorn porphyry deposits, Woodjam property, central British Columbia (Parts of 093A); *in* Geoscience BC Summary of Activities 2012, Geoscience BC, Report 2013-1, p. 79–90.

Dilles, J.H., Kent, A.J.R., Wooden, J.L., Tosdal, R.M., Koleszar, A., Lee, R.G., and Farmer, L.P., 2015. Zircon compositional evidence for sulphur-degassing from ore-forming arc magmas; Economic Geology, v. 110, no. 1, p. 241–251. https://doi.org/10.2113/econgeo.110.1.241

Drummond, A.D., Sutherland Brown, A., Young, R.J., and Tennant, S.J., 1976. Gibraltar – regional metamorphism, mineralization, hydrothermal alteration and structural development; *in* Porphyry deposits of the Canadian Cordillera, (ed.) A. Sutherland Brown; Canadian Institute of Mining and Metallurgy, Special Volume 15, p. 195–205.

Ferbey, T., Plouffe, A., and Bustard, A.L., 2016. Geochemical, mineralogical, and textural data from tills in the Highland Valley Copper mine area, south-central British Columbia; British Columbia Ministry of Energy and Mines, British Columbia Geological Survey, GeoFile 2016–11, 1 .zip file and Geological Survey of Canada, Open File 8119, 1 .zip file. https://doi.org/10.4095/299242

Garrett, R.G., 2013. The 'rgr' package for the R Open Source statistical computing and graphics environment - a tool to support geochemical data interpretation; Geochemistry: Exploration, Environment, Analysis, v. 13, p. 355–378. https://doi.org/10.1144/geochem2011-106

Grapes, R.H. and Hoskin, P.W.O., 2004. Epidote group minerals in low-medium pressure metamorphic terranes; Reviews in Mineralogy and Geochemistry, v. 56, no. 1, p. 301–345. https://doi.org/10.2138/gsrmg.56.1.301

Greenwood, H.J., Woodsworth, G.J., Read, P.B., Ghent, E.D., and Evenchick, C.A., 1991. Metamorphism; *in* Geology of the Cordilleran Orogen in Canada, (ed.) H. Gabrielse and C.J. Yorath; Geological Survey of Canada, Geology of Canada Series no. 4, p. 535–570. https://doi.org/10.4095/134107

Griffin, W.L., Powell, W.J., Pearson, N.J., and O'Reilly, S.Y., 2008. GLITTER: Data reduction software for laser ablation ICP–MS; *in* Laser ablation-ICP-mass spectrometry in the earth sciences: current practices and outstanding issues, (ed.) P. Sylvester; Mineralogical Association of Canada, Short Course Series, v. 40, p. 308–311.

Guillong, M., Hametner, K., Reusser, E., Wilson, S. A., and Günther, D., 2005. Preliminary characterisation of new glass reference materials (GSA-1G, GSC-1G, GSD-1G and GSE-1G) by laser ablation-inductively coupled plasma-mass spectrometry using 193 nm, 213 nm and 266 nm wavelengths; Geostandards and Geoanalytical Research, v. 29, n. 3, p. 315–331. https://doi.org/10.1111/j.1751-908X.2005.tb00903.x

Hashmi, S., Ward, B.C., Plouffe, A., Leybourne, M.I., and Ferbey, T., 2015. Geochemical and mineralogical dispersal in till from the Mount Polley Cu-Au porphyry deposit, central British Columbia, Canada; Geochemistry: Exploration, Environment, Analysis, v. 15, no. 2, p. 234–249. https://doi.org/10.1144/geochem2014-310

Hickin, A.S. and Plouffe, A., 2017. Sampling and interpreting stream, lake, and glacial sediments for mineral exploration in the Canadian Cordillera, a review; *in* Indicator minerals in till and stream sediments of the Canadian Cordillera, (ed.) T. Ferbey, A. Plouffe, and A.S. Hickin; Geological Association of Canada, Special Paper, v. 50 and Mineral Association of Canada, Topics in Mineral Sciences v. 47, p. 27–51.

Jago, C.P., Tosdal, R.M., Cooke, D.R., and Harris, A.C., 2014. Vertical and lateral variation of mineralogy and chemistry in the Early Jurassic Mt. Milligan alkalic porphyry Au-Cu deposit, British Columbia, Canada; Economic Geology, v. 109, no. 4, p. 1005–1033. https://doi.org/10.2113/econgeo.109.4.1005

Jochum, K.P., Nohl, U., Herwig, K., Lammel, E., Stoll, B., and Hofmann, A.W., 2005a. GeoReM : A new geochemical database for reference materials and isotopic standards. Geostandards and Geoanalytical Research, v. 29, p. 333–338. https://doi.org/10.1111/j.1751-908X.2005.tb00904.x

Jochum, K.P., Willbold, M., Raczek, I., Stoll, B., and Herwig, K., 2005b. Chemical characterisation of the USGS reference glasses GSA-1G, GSC-1G, GSD-1G, GSE-1G, BCR-2G, BHVO-2G and BIR-1G using EPMA, ID-TIMS, ID-ICP-MS and LA-ICP-MS; Geostandards and Geoanalytical Research, v. 29, p. 285–302. https://doi.org/10.1111/j.1751-908X.2005.tb00901.x

Kane, J.S., 1998. A history of the development and certification of NIST glass SRMs 610-617; Geostandards Newsletter, v. 22, p. 7–13. https://doi.org/10.1111/j.1751-908X.1998.tb00542.x

Kobylinski, C., Hattori, K., Plouffe, A., and Smith, S., 2017. Epidote associated with the porphyry Cu-Mo mineralization at the Gibraltar deposit, south central British Columbia; Geological Survey of Canada, Open File 8279, 19 p. https://doi.org/10.4095/305912

Liang, H.-Y., Campbell, I.H., Allen, C., Sun, W.-D., Liu, C.-Q., Yu, H.-X., Xie, Y.-W., and Zhang, Y.-Q., 2006. Zircon Ce4+/Ce3+ ratios and ages for Yulong ore-bearing porphyries in eastern Tibet; Mineralium Deposita, v. 41, 152. https://doi.org/10.1007/s00126-005-0047-1

Logan, J.M., 2013. Porphyry systems of central and southern BC: Overview and field trip road log; in Porphyry systems of central and southern British Columbia: tour of central British Columbia porphyry deposits from Prince George to Princeton, (ed.) J.M. Logan and T.G. Schroeter; Society of Economic Geologists, Field Trip Guidebook, Series 44, p. 1–45.

Logan, J.M. and Mihalynuk, M.G., 2014. Tectonic controls on Early Mesozoic paired alkaline porphyry deposit belts (Cu-Au±Ag-Pt-Pd-Mo) within the Canadian Cordillera; Economic Geology, v. 109, p. 827–858. https://doi.org/10.2113/econgeo.109.4.827

Logan, J.M. and Schroeter, T.G. (ed.), 2013. Porphyry systems of central and southern British Columbia: tour of central British Columbia porphyry deposits from Prince George to Princeton; Society of Economic Geologists, Field Trip Guidebook, Series 44, 143 p.

Logan, J.M., Schiarizza, P., Struik, L.C., Barnett, C., Nelson, J.L., Kowalczyk, P., Ferri, F., Mihalynuk, M.G., Thomas, M.D., Gammon, P., Lett, R., Jackaman, W., and Ferbey, T., (comp.), 2010. Bedrock geology of the QUEST map area, central British Columbia; Geoscience BC Report 2010-5, British Columbia Geological Survey Geoscience Map 2010-1 and Geological Survey of Canada Open File 6476, 1 sheet, scale 1:500 000. https://doi.org/10.4095/261517

Lowell, J.D. and Guilbert, J.M., 1970. Lateral and vertical alteration-mineralization zoning in porphyry ore deposits; Economic Geology, v. 65, no. 4, p. 373–408. https://doi.org/10.2113/gsecongeo.65.4.373

Mao, M., Rukhlov, A.S., Rowins, S.M., Hickin, A.S., Ferbey, T., Bustard, A.L., Spence, J., and Coogan, L.A., 2017. A novel approach using detrital apatite and till geochemistry to identify covered mineralization in the TREK area of the Nechako Plateau, British Columbia; *in* Indicator minerals in till and stream sediments of the Canadian Cordillera, (ed.) T. Ferbey, A. Plouffe, and A.S. Hickin; Geological Association of Canada, Special Paper, v. 50 and Mineral Association of Canada, Topics in Mineral Sciences, v. 47, p. 191–243.

Massey, N.W.D., MacIntyre, D.G., Desjardins, P.J., and Cooney, R.T., 2005. Geology of British Columbia; British Columbia Ministry of Energy, Mines and Petroleum Resources, British Columbia Geological Survey, Geoscience map 2005-3, scale 1:1 000 000.

McMillan, W.J. and Panteleyev, A., 1995. Porphyry copper deposits of the Canadian Cordillera; *in* Porphyry copper deposits of the American Cordillera, (ed.) F.W. Pierce and J.G. Bolm; Arizona Geological Society, Digest 20, p. 203–218.

McMillan, W.J., Thompson, J.F.H., Hart, C.J.R., and Johnston, S.T., 1995. Regional geological and tectonic setting of porphyry deposits in British Columbia and Yukon Territory; *in* Porphyry deposits of the northwestern Cordillera of North America, (ed.) T.G. Schroeter; Canadian Institute of Mining, Metallurgy and Petroleum, Special Volume 46, p. 40–57.

McMillan, W.J., Thompson, J.F.H., Hart, C.J.R., and Johnston, S.T., 1996. Porphyry deposits of the Canadian Cordillera; Geoscience Canada, v. 23, no. 3, p. 125–134.

Mihalasky, M.J., Bookstrom, A.A., Frost, T.P., and Ludington, S., with contributions from Logan, J.M., Panteleyev, A., and Abbott G., 2011. Porphyry copper assessment of British Columbia and Yukon Territory, Canada; United States Geological Survey, Scientific Investigations Report 2010-5090-C, 128 p.

Mills, S.J., Hatert, F., Nickel, E.H., and Ferraris, G., 2009. The standardisation of mineral group hierarchies: application to recent nomenclature proposals; European Journal of Mineralogy, v. 21, no. 5, p. 1073–1080. https://doi.org/10.1127/0935-1221/2009/0021-1994

Norman, D.K., Parry, W.T., and Bowman, J.R., 1991. Petrology and geochemistry of propylitic alteration at southwest Tintic, Utah; Economic Geology, v. 86, no. 1, p. 13–28. https://doi.org/10.2113/gsecongeo.86.1.13

Pacey, A., Wilkinson, J.J., and Cooke, D.R., 2020. Chlorite and epidote mineral chemistry in porphyry ore systems: a case study of the Northparkes District, NSW, Australia; Economic Geology, v. 115, no. 4, p. 701–727. https://doi.org/10.5382/econgeo.4700

Panteleyev, A., Bailey, D.G., Bloodgood, M.A., and Hancock, K.D., 1996. Geology and mineral deposits of the Quesnel River-Horsefly map area, central Quesnel Trough, British Columbia; British Columbia Ministry of Employment and Investment, British Columbia Geological Survey, Bulletin 97, 156 p.

Plouffe, A. and Ferbey, T., 2015a. Surficial geology, Granite Mountain area, British Columbia, parts of NTS 93-B/8 and 93-B/9; Geological Survey of Canada, Canadian Geoscience Map 223 (preliminary edition) and British Columbia Geological Survey, Geoscience Map 2015-4, scale 1:50 000. https://doi.org/10.4095/296793

Plouffe, A. and Ferbey, T., 2015b. Till composition near Cu-porphyry deposits in British Columbia: highlights for mineral exploration; *in* TGI 4 – Intrusion related mineralisation project: new vectors to buried porphyry-style mineralisation, (ed.) N. Rogers; Geological Survey of Canada, Open File 7843, p. 15–37. https://doi.org/10.4095/296464

Plouffe, A. and Ferbey, T., 2016. Till geochemistry, mineralogy and textural data near four Cu porphyry deposits in British Columbia; Geological Survey of Canada, Open File 8038 and British Columbia Geological Survey, Geofile 2016-10, 44 p. https://doi.org/10.4095/298805

Plouffe, A. and Ferbey, T., 2017. Porphyry Cu indicator minerals in till: A method to discover buried mineralisation; *in* Indicator minerals in till and stream sediments of the Canadian Cordillera, (ed.) T. Ferbey, A. Plouffe, and A. Hickin; Geological Association of Canada, Special Paper v. 50 and Mineral Association of Canada, Topics in Mineral Sciences, v. 47), p. 129–159.

Plouffe, A., Bednarski, J.M., Huscroft, C.A., Anderson, R.G., and McCuaig, S.J., 2011. Late Wisconsinan glacial history in the Bonaparte Lake map area, south central British Columbia: implications for glacial transport and mineral exploration; Canadian Journal of Earth Sciences, v. 48, no. 6, p. 1091–1111. https://doi.org/10.1139/e10-100

Plouffe, A., Ferbey, T., Hashmi, S., and Ward, B.C., 2016. Till geochemistry and mineralogy: vectoring towards Cu porphyry deposits in British Columbia, Canada; Geochemistry: Exploration, Environment, Analysis, v. 16, no. 3–4, p. 213–232. https://doi.org/10.1144/geochem2015-398

Plouffe, A., Kobylinski, C.H., Hattori, K., Wolfe, L., and Ferbey, T., 2018. Mineral markers of porphyry copper mineralisation: work in progress at the Gibraltar deposit, British Columbia; *in* Targeted Geoscience Initiative: 2017 report of activities, volume 1, (ed.) N. Rogers; Geological Survey of Canada, Open File 8358, p. 57–67. https://doi.org/10.4095/306423

Plouffe, A., Kjarsgaard, I.M., Kobylinski, C., Hattori, K., Petts, D.C., Venance, K.E., and Ferbey, T., 2019. Discovering the next generation of copper porphyry deposits using mineral markers; *in* Targeted Geoscience Initiative: 2018 report of activities, (ed.) N. Rogers; Geological Survey of Canada, Open File 8549, p. 321–331. https://doi.org/10.4095/313666

R Core Team, 2018. R. A language and environment for statistical computer; R Foundation for Statistical Computer, Vienna, Austria. http//www.r-project.org [accessed March 25, 2020]

Read, P.B., Woodsworth, G.J., Greenwood, H.J., Ghent, E.D., and Evenchick, C.A., 1991. Metamorphic map of the Canadian Cordillera; Geological Survey of Canada, Map 1714A, scale 1:2 000 000. https://doi.org/10.4095/134142

Rees, C., 2013. The Mount Polley Cu-Au deposit, south-central British Columbia, Canada; *in* Porphyry systems of central and southern British Columbia: tour of central British Columbia porphyry deposits from Prince George to Princeton, (ed.) J.M. Logan and T.G. Schroeter; Society of Economic Geologists, Field Trip Guidebook, Series 44, p. 67–98.

Schiarizza, P., 2016. Toward a regional stratigraphic framework for the Nicola Group: preliminary results from the Bridge Lake – Quesnel River area; *in* Geological Fieldwork 2015, British Columbia Ministry of Energy, Mines and Petroleum Resources, British Columbia Geological Survey, Paper 2016-1, p. 13–30.

Schiarizza, P., 2019. Geology of the Nicola Group in the Bridge Lake-Quesnel River area, south-central British Columbia; *in* Geological Fieldwork 2018, British Columbia Ministry of Energy, Mines and Petroleum Resources, British Columbia Geological Survey, Paper 2019-01, p. 15–30.

Schroeter, T.G., (ed.), 1995. Porphyry deposits of the northwestern Cordillera of North America; Canadian Institute of Mining, Metallurgy and Petroleum, Special Volume 46, 888 p.

Shen, P., Hattori, K., Pan, H., Jackson, S., and Seitmuratova, E., 2015. Oxidation condition and metal fertility of granitic magmas: zircon trace-element data from porphyry Cu deposits in the central Asian orogenic belt; Economic Geology, v. 110, no. 7, p. 1861–1878. https://doi.org/10.2113/econgeo.110.7.1861

Sherlock, R. and Trueman, A., 2013. NI 43-101 technical report for 2012 activities on the Woodjam South property; Gold Fields Horsefly Exploration Group and Consolidated Woodjam Copper Corporation, Cariboo Mining Division, British Columbia, 158 p.

Sherlock, R., Blackwell, J., and Skinner, T., 2013. NI 43-101 technical report for 2012 activities on the Woodjam North property; Gold Fields Horsefly Exploration Group, Consolidated Woodjam Copper Corporation, Cariboo Mining Division, British Columbia, 275 p.

Sillitoe, R.H., 2010. Porphyry copper systems; Economic Geology, v. 105, no. 1, p. 3–41. https://doi.org/10.2113/gsecongeo.105.1.3

Sinclair, W.D., 2007. Porphyry deposits; *in* Mineral deposits of Canada: a synthesis of major deposit types, district metallogeny, the evolution of geological provinces, and exploration methods, (ed.) W.D. Goodfellow; Geological Association of Canada, Mineral Deposit Division, Special Publication No. 5, p. 223–243.

Sutherland Brown, A.E., (ed.), 1976. Porphyry deposits of the Canadian Cordillera; Canadian Institute of Mining and Metallurgy, Special Volume 15, 510 p.

Sylvester, P.J., Cabri, L.J., Tubrett, M.N., Peregoedova, A., McMahon, G., and Laflamme, J.H.G., 2005. Synthesis and evaluation of a fused pyrrhotite standard reference material for platinum group element and gold analysis by laser ablation–ICPMS; *in* Platinum-group elements from genesis to beneficiation and environmental impact, (ed.) T.O. Törmänen and T.T. Alapieti; Geological Survey of Finland, 10th International Platinum Symposium, Oulu, Finland, p. 16–20, extended abstracts.

Taseko Mines Ltd., 2020. Taseko Mines Limited. <www.tasekomines.com> [accessed March 2020]

Thió-Henestrosa, S. and Martín-Fernández, J., 2005. Dealing with compositional data: the freeware CoDaPack; Mathematical Geosciences, v. 37, p. 773–793. https://doi.org/10.1007/s11004-005-7379-3

van Straaten, B.I., Oliver, J., Crozier, J., and Goodhue, L., 2013. A summary of the Gibraltar porphyry copper-molybdenum deposit, south-central British Columbia, Canada; *in* Porphyry systems of central and southern British Columbia: tour of central British Columbia porphyry deposits from Prince George to Princeton, (ed.) J.M. Logan and T.G. Schroeter; Society of Economic Geologists, Field Trip Guidebook, Series 44, p. 55–66.

Wilkinson, J.J., Baker, M.J., Cooke, D.R., Wilkinson, C.C., and Inglis, S., 2017a. Exploration targeting in porphyry Cu systems using propylitic mineral chemistry: a case study of the El Teniente deposit, Chile; *in* Mineral resources to discover, volume 3, proceedings of the 14th Biennial Society of Geology Applied to Mineral Deposits meeting, (ed.) P. Mercier-Langevin; Society of Geology Applied to Mineral Deposits, p. 1111–1115.

Wilkinson, J.J., Cooke, D.R., Baker, M.J., Chang, Z., Wilkinson, C.C., Chen, H., Fox, N., Hollings, P., White, N.C., Gemmell, J.B., Loader, M.A., Pacey, A., Sievwright, R.H., Hart, L.A., and Brugge, E.R., 2017b. Porphyry indicator minerals and their mineral chemistry as vectoring and fertility tools; *in* Application of indicator mineral methods to bedrock and sediments, (ed.) M.B. McClengaghan and D. Layton-Matthews; Geological Survey of Canada, Open File 8345, p. 67–77. https://doi.org/10.4095/306317

APPENDIX A

Laser-ablation inductively coupled plasma mass spectrometry analytical results of epidote

The complete list of laser-ablation inductively coupled plasma mass spectrometry analytical results of major, minor, and trace-element concentrations in epidote are found in the file:POR-08_Appendix A.xlsx. Values are in parts per million (ppm). Analytical results of standard samples are included on separate worksheets. The table contains basic information on sample type and location. *See* text for analytical details. This Appendix has not been edited to Geological Survey of Canada specifications.